

Prioritization of non-coding elements involved in non-syndromic cleft lip with/without cleft palate through genome-wide analysis of *de novo* mutations

Hanna K. Zieger,¹ Leonie Weinhold,² Axel Schmidt,¹ Manuel Holtgrewe,³ Stefan A. Juranek,⁴ Anna Siewert,¹ Annika B. Scheer,¹ Frederic Thieme,¹ Elisabeth Mangold,¹ Nina Ishorst,¹ Fabian U. Brand,⁵ Julia Welzenbach,¹ Dieter Beule,^{3,6} Katrin Paeschke,⁴ Peter M. Krawitz,² and Kerstin U. Ludwig^{1,*}

Summary

Non-syndromic cleft lip with/without cleft palate (nsCL/P) is a highly heritable facial disorder. To date, systematic investigations of the contribution of rare variants in non-coding regions to nsCL/P etiology are sparse. Here, we re-analyzed available whole-genome sequence (WGS) data from 211 European case-parent trios with nsCL/P and identified 13,522 *de novo* mutations (DNMs) in nsCL/P cases, 13,055 of which mapped to non-coding regions. We integrated these data with DNMs from a reference cohort, with results of previous genome-wide association studies (GWASs), and functional and epigenetic datasets of relevance to embryonic facial development. A significant enrichment of nsCL/P DNMs was observed at two GWAS risk loci (4q28.1 ($p = 8 \times 10^{-4}$) and 2p21 ($p = 0.02$)), suggesting a convergence of both common and rare variants at these loci. We also mapped the DNMs to 810 position weight matrices indicative of transcription factor (TF) binding, and quantified the effect of the allelic changes *in silico*. This revealed a nominally significant overrepresentation of DNMs ($p = 0.037$), and a stronger effect on binding strength, for DNMs located in the sequence of the core binding region of the TF Musculin (MSC). Notably, MSC is involved in facial muscle development, together with a set of nsCL/P genes located at GWAS loci. Supported by additional results from single-cell transcriptomic data and molecular binding assays, this suggests that variation in MSC binding sites contributes to nsCL/P etiology. Our study describes a set of approaches that can be applied to increase the added value of WGS data.

Introduction

Non-syndromic cleft lip with/without cleft palate (nsCL/P) is the most frequent form of orofacial clefting (OFC), with an estimated prevalence of 1 in 1,000 European newborns.¹ Depending on severity, nsCL/P treatment requires multidisciplinary approaches, including repeated surgeries, throughout childhood and adolescence. Together with an increased life-time risk for morbidity and mortality,² nsCL/P represents a major burden for affected individuals and their families.

NsCL/P has a multifactorial etiology, and estimates from twin studies suggest a heritability of ~90%.³ Recent genome-wide association studies (GWASs) have identified common risk variants at 45 genomic loci, which explain about 30% of phenotypic variance in Europeans.⁴ Research suggests that further types of genetic variation may also contribute to disease risk, including variants from the low-frequency part of the allelic spectrum. For example, previous studies have identified private and rare risk variants for nsCL/P in genes underlying orofacial cleft syndromes within multiplex families,⁵ in genes involved in epithelial cell adhesion processes,⁶ and in genes located within GWAS loci.^{7–10} In a recent multiethnic study of

several hundred case-parent trios of OFC (Bishop et al.),¹¹ potentially causal *de novo* mutations (DNMs) in protein-coding regions were investigated using data from whole-genome sequencing (WGS). The cohort included individuals with cleft lip with/without cleft palate (CL/P), including its subtypes cleft lip only (CLO) as well as cleft lip and palate (CLP), and cleft palate only (CPO). In that study, the authors identified a cohort-wide enrichment of loss of function (LoF) DNMs, in particular in genes expressed in human neural crest cells (hNCCs). At the individual gene level, this study also implicated *TFAP2A* (MIM: 107580), *IRF6* (MIM: 607199), and *ZFH4* (MIM: 606940) in OFC etiology.¹¹

To date, most analyses of systematic sequencing data (including Bishop et al.) have been limited to protein-coding regions, mainly because of the comparable ease of functional annotation and etiological interpretation for coding variants. In contrast, few data are available concerning the contribution of rare variants or DNMs located in non-coding regions. Evidence that non-coding variants are involved in nsCL/P has been generated by studies that identified causal non-coding mutations in individual pedigrees,^{10,12,13} and reports of a burden of low-frequency variants in non-coding enhancer regions that are active in

¹Institute of Human Genetics, University of Bonn, School of Medicine and University Hospital Bonn, Bonn 53127, Germany; ²Institute for Medical Biometry, Informatics and Epidemiology, University Hospital Bonn, Bonn 53127, Germany; ³Core Unit Bioinformatics, Berlin Institute of Health, Berlin 10117, Germany; ⁴Department of Oncology, Hematology and Rheumatology, University Hospital Bonn, Bonn 53127, Germany; ⁵Institute for Genomic Statistics and Bioinformatics, University Hospital Bonn, Bonn 53127, Germany; ⁶Max Delbrück Center for Molecular Medicine, Berlin 13125, Germany

*Correspondence: kerstin.ludwig@uni-bonn.de

<https://doi.org/10.1016/j.xhgg.2022.100166>.

© 2022 The Authors. This is an open access article under the CC BY-NC-ND license (<http://creativecommons.org/licenses/by-nc-nd/4.0/>).



developing craniofacial tissue.^{14,15} The aim of the present study was to identify etiologically relevant DNMs for nsCL/P, with a focus on strategies to prioritize DNMs in non-coding regions.

Material and methods

This study used prior published data, no human or animal subjects were involved. Respective datasets were analyzed upon approved data access and following the criteria laid out in the respective data use agreements in the NIH database of Genotypes and Phenotypes (dbGaP). Informed consent and ethical approval were obtained by the investigators of the original studies. The molecular and computational studies did not involve any human material. All procedures followed biological safety and ethics standards.

Subjects and data resources

WGS raw sequence and phenotypic data for 1,236 individuals from a European OFC cohort were retrieved from the Gabriella Miller Kids First (GMKF) Project, upon approved access (section “Web resources”). Based on available pedigree information, 220 complete parent-offspring pairs (“trios”) containing both unaffected parents and a child with nsCL/P were identified. Additionally, a set of 330 trios with children being affected by Ewing sarcoma (ES) was obtained from GMKF. This cohort was used as a non-cleft reference (NCR) cohort. Further information can be found in the [supplemental methods](#).

WGS data analysis and variant calling

For each individual, WGS reads were aligned to GRCh37, and variant calling was performed using both Unified Genotyper and Haplotype Caller. To generate a high-quality variant DNM call set, data processing required the complete absence of reads in any parent, and support of variant calls by both calling algorithms ([supplemental methods](#)). All DNMs were annotated with information (1) on frequency (gnomAD v3.1, all populations), (2) on genomic location (exonic, intronic, intergenic; based on GENCODE Basic gene annotation version33.hg19), and (3) with each of six *in silico* prediction scores that are applicable to both non-coding and coding variants: CADD,¹⁶ ReMM,¹⁷ FATHMM,¹⁸ DANN,¹⁹ LINSIGHT,²⁰ and nER²¹ ([supplemental methods](#)). No general frequency filter was applied ([Figure S1](#)). As our nsCL/P cohort represents a subcohort of Bishop et al. that was analyzed using a different quality control (QC) and variant calling pipeline, coding DNMs were compared between both studies, based on available information (Table S3 by Bishop et al., participant IDs provided by GMKF) and annotations provided by the Ensembl Variant Effect Predictor²² (VEP; section “web resources”).

The statistical comparison of DNM distribution between nsCL/P and NCR included the average number of DNMs per sample (Mann-Whitney U (MWU) test for total DNMs and subgroups of exonic, intronic, and intergenic DNMs), the distribution of *in silico* prediction scores for nsCL/P and NCR DNMs, and the proportion of DNMs with *in silico* prediction scores over individual or combined thresholds ([supplemental methods](#)).

Analysis of DNM enrichment in genomic features

To study the enrichment of DNMs across the entire genome, diverse genomic datasets were retrieved. For each of those datasets, DNM enrichment was calculated using the R package FunciVar,²³

which compares inter-cohort enrichment probabilities for functional elements using a Bayesian approach (see FunciVar in section “web resources,” [supplemental methods](#)). The datasets included genome-wide maps of eight chromatin states from hNCCs,²⁴ cranial neural crest cells (cNCCs),²⁵ and human facial embryonic tissues,²⁶ which had been aggregated in a previous study by our group.⁴ Furthermore, general genomic features with *a priori* evidence for functional relevance or evolution were included; i.e., (1) 4,307 evolutionarily highly conserved non-coding elements (CNEs) based on a prior publication,²⁷ and (2) 1,570 enhancer regions from the VISTA enhancer browser²⁸ ([supplemental methods](#)).

Analysis of topologically associating domains

To detect local enrichments of non-coding DNMs independent of genomic features (comparable with gene-burden tests for protein-coding variants), DNMs were combined based on their location within regulatory units; i.e., topologically associating domains (TADs). Positional data were retrieved for 2,991 TADs from human embryonic stem cells, as described elsewhere,⁴ and enrichment of DNMs in TADs was tested using FunciVar ([supplemental methods](#)). Given the considerable burden of multiple testing with regard to the present sample size, we additionally defined a set of 45 candidate TADs on the basis of recent GWAS results, as previously described⁴ (TADs_{GWAS}, [Table S1](#)).

Analysis of DNMs in TF binding sites

Position weight matrix (PWM) information representing 810 transcription factor binding site (TFBS) motifs was retrieved from JASPAR2020.²⁹ Using a modified version of a previously published pipeline (see denovoLOBGOB, sections “Web resources,” “data and code availability”), changes in transcription factor (TF) binding between reference and alternative alleles were qualitatively predicted and quantified for each DNM (after excluding insertions/deletions (indels); n = 28,773 DNMs). Statistical analyses of individual PWMs were performed to determine (1) differences in how frequently a specific PWM matches the genomic region around the DNMs (Fisher’s exact test), and (2) quantitative differences in predicted binding strength (MWU test). For the latter, for each DNM, the effect of the variant allele was calculated as described above, and the difference from the reference allele was determined as an absolute change of binding. Then, absolute change values were combined for all DNMs of one PWM and compared between the two cohorts. In addition, for each analysis (1) and (2), log₂-fold changes (log₂FC) between nsCL/P and NCR were calculated. Further information can be found in the [supplemental methods](#).

Single-cell expression data

Single-cell expression data obtained from murine embryos were downloaded from (1) the Mouse Organogenesis Cell Atlas (MOCA), which includes a time series of developmental organogenesis from E9.5 to E13.5 (section “Web resources”); and (2) the lambda-doid junction at day E11.5, which represents the time point for the fusing of facial structures.³⁰ Both datasets were re-analyzed using a joint in-house computational pipeline ([supplemental methods](#)).

Electrophoretic mobility shift assays

For each of the DNMs observed within MSC binding sites, gain or loss of binding was predicted based on the allelic change within the motif: gain of binding (if PWM-ref < PWM-alt), loss of binding (PWM-ref > PWM-alt), and silent effects (PWM-ref = PWM-alt).

Table 1. Distribution of DNMs in nsCL/P and NCR trios

	nsCL/P	NCR	Combined
Total DNMs	13,522	17,968	31,490
SNVs	12,335	16,438	28,773
Small insertions/deletions	1,187	1,530	2,717
Protein-coding DNMs ^a	222 (1.05) ^c	338 (1.19) ^c	560
LoF DNMs ^b	22 (0.10) ^c	19 (0.07) ^c	41
Nonsense DNMs	10	11	21
Frameshift DNMs	12	8	20
Missense DNMs	129 (0.61) ^c	246 (0.87) ^c	375
Synonymous DNMs	71 (0.34) ^c	73 (0.26) ^c	144

DNMs, *de novo* mutations; nsCL/P, non-syndromic cleft lip with/without cleft palate; NCR, non-cleft reference cohort; LoF, loss of function.

^aExonic DNMs based on GENCODE Basic gene annotation version33.hg19, including non-coding parts of gene sequences (e.g., 3'/5' UTRs).

^bEffect combinations from Variant Effect Predictor output were reduced to classes (see Table S4 for grouped effect names). LoF DNMs include nonsense and frameshift DNMs.

^cIn brackets: relative frequency of this type of DNM in the respective cohort.

Then, five candidate binding sites were selected from the set of DNMs; i.e., two motifs located at nsCL/P DNMs with either the strongest loss (chromosome [chr.] 6, chr. 10) or strongest gain (chr. 7, chr. 16), and the motif with the strongest predicted binding change by DNM in NCR (chr. 5; Table S2). For each of the five candidate binding sites of MSC, the genomic context around the DNM (i.e., an additional 20 bp up- and downstream) was retrieved. Each target oligonucleotide was designed with the respective duplex reference and alternative motif, and each contained p³² marks at the 5' end of the top strand. Following cloning of MSC into the pET-28a vector, expression in *Escherichia coli*, and purification, the protein was incubated with binding buffer and oligonucleotides, for 30 min. Then 10 nM DNA was incubated with five different concentrations of MSC (range 0–1 μM). Binding effects were monitored according to the presence of protein-oligo dimers at predicted molecular size on native gels, and potential allele-specific effects were indicated by gel mobility changes (supplemental methods, all tested sequences in Table S2). All analyses were performed in triplicate.

Results

High-confidence variant set of coding and non-coding DNMs

After sample- and variant QC (Figures S2, S3, and S4), the final dataset contained 211 nsCL/P trios (52 of which were CLO, and 159 CLP; Figures S5 and S6), 284 NCR trios, and 31,490 autosomal DNMs (13,522 in nsCL/P; 17,968 in NCR; Table 1). Among those, 28,773 DNMs were single-nucleotide variants (SNVs), and 2,717 were small indels. Sixteen DNMs were recurrent (four within nsCL/P, seven within NCR, and five were observed in both cohorts; Table S3). Overall, an average of 63.6 autosomal DNMs was observed per trio, consistent with expectations.³¹ No significant difference in the average number of DNMs was observed between nsCL/P and NCR trios (64.1 versus 63.3; $p = 0.47$; Figure S7), and both cohorts showed a similar distribution of DNMs across exonic, intronic, and intergenic regions (Figure 1A).

Within the nsCL/P cohort, 222 of the exonic DNMs mapped within protein-coding sequences according to VEP (Tables 1, S4, and S5; supplemental methods). This included 22 LoF (12 frameshift, 10 nonsense), 129 missense (together denoted as protein-altering DNMs), and 71 synonymous variants. No splice site DNM was observed. Notably, 159 of the 222 coding DNMs were previously reported by Bishop et al. (=71.6%, supplemental methods). This indicates convergence of the identified DNMs between both studies, taking into account the differences in variant calling pipelines and quality parameters. An aggregation of all coding DNMs of this study and the study by Bishop et al. can be found in Table S6.

Identification of deleterious variants in craniofacial genes

We next annotated each of the 31,490 DNMs with six *in silico* prediction scores (i.e., CADD, ReMM, FATHMM, DANN, LINSIGHT, and ncER). Comparison of score distributions did not reveal conclusive differences between nsCL/P and NCR (Figures 1B, S8, S9, and S10; Tables S7, S8, S9, S10, S11, S12, S13, and S14), and filtering for DNMs with CADD ≥ 20 did not show a significant difference between cohorts ($p = 0.18$, 144 DNMs in nsCL/P [1.06%], 226 DNMs in the NCR cohort [1.26%]; Table S15). Notably, DNMs in numerous craniofacial genes, such as *WNT4* (MIM: 603490),^{32,33} *ALPI* (MIM: 171740),³⁴ and *MYO10* (MIM: 601481)^{35–37} were observed with high CADD scores of ≥ 30 in nsCL/P. In addition, one DNM (CADD score of 45) was observed in *PLEKHA6* (MIM: 607771), which is a paralog of *PLEKHA7* (MIM: 612686). Pathogenic variants in *PLEKHA7* were reported in a previous investigation of multiply affected nsCL/P families⁶; thereby, this result further supports the role of the PLEKHA-family in nsCL/P etiology.

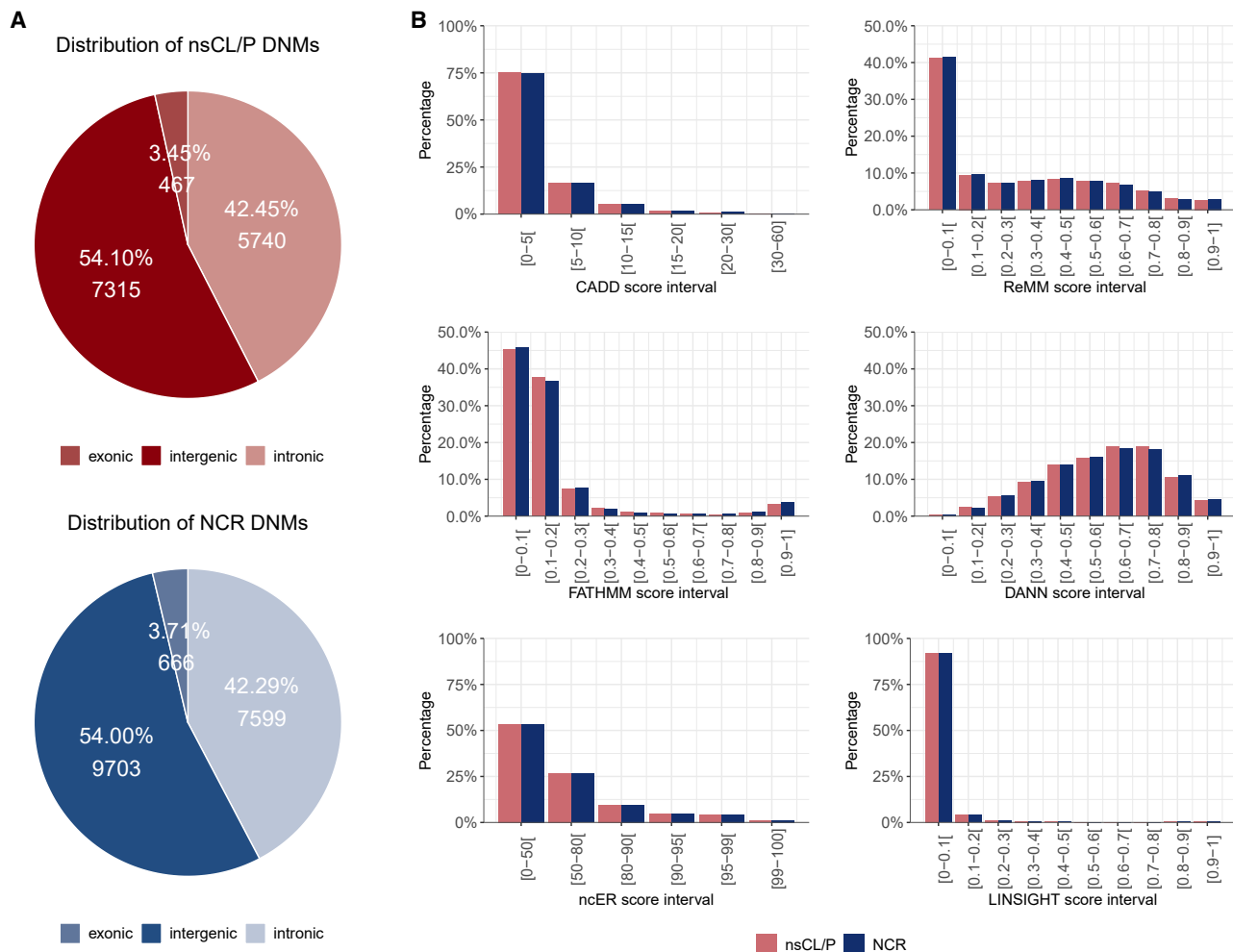


Figure 1. Comparative analyses of *de novo* mutations

(A) *De novo* mutations (DNMs) observed in non-syndromic cleft lip with/without cleft palate (nsCL/P) case-parent trios (red) and NCR trios (blue) were annotated according to genomic location (i.e., exonic/intronic/intergenic). Exonic DNMs were defined based on exons of protein-coding genes in the GENCODE Basic gene annotation version33.hg19, including non-coding parts of gene sequences (e.g., 3'/5' UTRs). DNMs were equally distributed between the two cohorts.

(B) DNMs were annotated with each of six distinct *in silico* prediction scores, and their distribution was compared between the two cohorts. No significant differences were found.

Limited evidence for enrichment of non-coding DNMs in genomic features

We first tested the hypothesis that DNMs are significantly enriched in epigenetic and functional datasets of relevance to embryonic facial development. No analysis-wide enrichment was observed, with the exception of a nominal significant finding in bivalent/poised transcription start sites and bivalent enhancers of Carnegie stage 15 of human facial embryonic tissue²⁶ (74 DNMs [0.55%; Table S16] in nsCL/P versus 68 DNMs in the NCR cohort [0.38%], $p = 0.03$; Figure 2A; Table S17). While this enrichment is noteworthy, the failure of reaching robust levels of statistical evidence precludes a conclusive statement.

No enrichment was observed for 34 nsCL/P DNMs that mapped to any of 4,307 CNEs (Figure 2B, 15 in nsCL/P versus 19 in NCR cohort; Tables S18, S19, and S20; $p = 0.88$). Regarding the 40 DNMs mapping to VISTA enhancers, again, no significant difference was observed

between the nsCL/P and NCR cohorts (14 versus 26; $p = 0.31$; Tables S21 and S22). This finding remained unchanged when DNMs were grouped for tissue-specific effects (activity in 16 of 23 different tissue types; Figure 2B; Table S23). Furthermore, no nsCL/P DNM was localized in both a CNE and a VISTA enhancer.

Convergence of non-coding DNMs at two GWAS risk loci

As TADs are considered the general regulatory units of the genome,³⁸ the aggregation of DNMs within its boundaries provides a systematic approach to aggregate DNMs with similar mechanistic effects. Based on the overall variant dataset, 29,629 DNMs were unambiguously mapped within 2,961 individual TADs (supplemental methods). While there was no test-wide significant difference between nsCL/P and NCR in terms of enrichment or depletion of DNMs in any of these TADs, we observed that 174 of the individual TADs showed a nominally significant

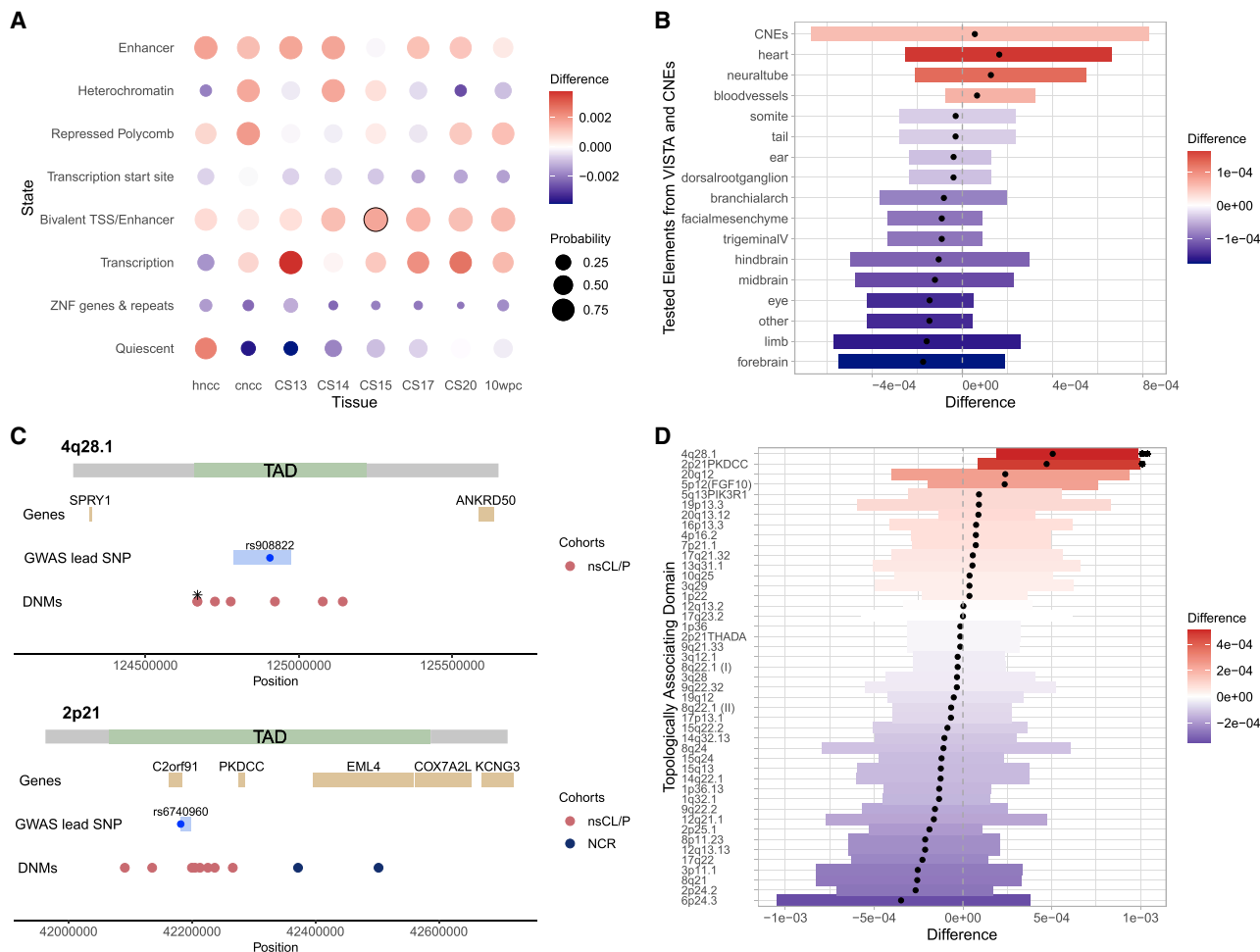


Figure 2. Enrichment of non-syndromic cleft lip with/without cleft palate *de novo* mutations in genomic candidate regions

(A) DNMs were mapped in eight chromatin states derived from human neural crest cells (hNCCs), cranial neural crest cells (cNCCs), and human embryonic facial tissue. FunciVar enrichment results are indicated by dot color. Dot sizes illustrate enrichment probabilities (increasing values represent increased statistical significance), and significant findings are encircled.

(B) Non-coding elements with previous evidence for functional relevance were retrieved from conserved non-coding elements (CNEs) and enhancer activity assays from VISTA ($n=16$ tissues). DNMs mapping to these regions were tested for enrichment in nsCL/P using FunciVar, similar to (A), and enrichment was depicted with their respective 95% credible interval (dots indicate median). The gray dashed line indicates a difference of zero.

(C) DNMs were mapped within boundaries of topologically associating domains (TADs), and a subset of 45 TADs was defined based on the presence of associated common nsCL/P risk variants (TAD_{GWAS}). Two loci (4q28.1, 2p21_{PKDCC}, see panel D) carried significantly more DNMs in nsCL/P. TAD boundaries are highlighted in green, with surrounding regions in gray. Gene locations are shown in yellow, together with GWAS-SNPs (dot) and GWAS credible SNP regions (bar) in blue. The positions of DNMs are indicated in red for nsCL/P and dark blue for NCR cohort. Two superimposed DNMs at 4q28.1 are indicated by an asterisk (*).

(D) Same graphical depiction as in (B), except for the TADs located at the 45 nsCL/P GWAS risk loci. Nominal significant p values are indicated with an asterisk (*), and p values significant after correction for 45 tests are indicated by a double asterisk (**).

enrichment ($n = 98$) or depletion ($n = 76$) of DNMs in nsCL/P compared with NCR (Table S24). Restricting the analysis to 45 TAD_{GWAS}, we observed 544 DNMs in total (221 nsCL/P versus 323 NCR), with two TAD_{GWAS} showing significant enrichment of DNMs in nsCL/P; i.e., 2p21_{PKDCC}³⁹ and 4q28.1⁴⁰ (Figure 2C; Tables S25 and S26). At the 4q28.1 locus, seven DNMs were observed in seven different individuals with nsCL/P, while no DNM in this region was observed in the NCR cohort ($p = 8 \times 10^{-4}$). At the 2p21_{PKDCC} locus, eight DNMs were observed in seven nsCL/P individuals and two DNMs in the NCR cohort ($p = 0.02$). Notably, the eight DNMs in

nsCL/P clustered within 175 kb around the GWAS lead variant rs6740960. The enrichment at the 4q28.1 locus remained significant after correction for multiple testing for the number of TAD_{GWAS} (Figure 2D). No TAD_{GWAS} showed a significant depletion of nsCL/P DNMs. These results suggest at least two loci where both common and rare variants may contribute to nsCL/P risk, at 2p21_{PKDCC} presumably through regulatory effects on *PKDCC* (MIM: 614150).^{41,42}

Identification of candidate TFs

Analyses were performed to test the hypothesis that DNMs contributing to nsCL/P might converge into

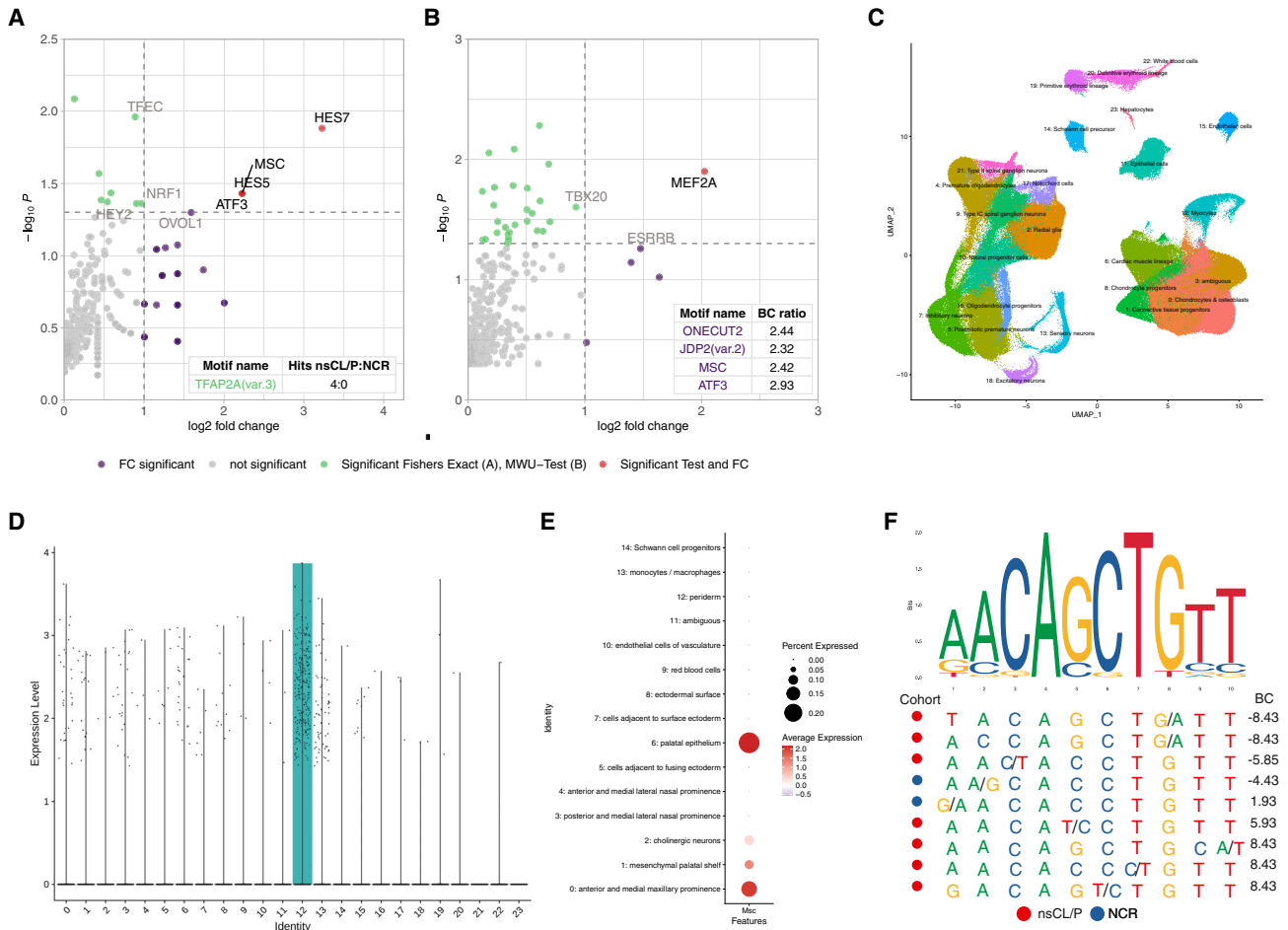


Figure 3. Identification of Musclin as a player in non-syndromic cleft lip with/without cleft palate etiology

(A) Qualitative analysis of DNMs in transcription factor (TF) binding sites (TFBS). Using 810 position weight matrices from JASPAR2020, the relative enrichment of non-syndromic cleft lip with/without cleft palate (nsCL/P) DNMs was assessed using \log_2FC (on y axis) versus Fisher's exact tests ($-\log_{10}(p$ value) on x axis). Insert represents motif TFAP2a (var.3) that had $\log_2FC \geq 1$ but lacked observations in the control cohort.

(B) Quantitative assessment of allelic effects on TF binding. For each DNM, the binding change (BC) of alternative versus reference allele was assessed via the Mann-Whitney U (MWU) test (on x axis) and \log_2FC (on y axis, calculated using the ratio of mean change of binding between cohorts). All motifs with ≥ 3 hits per cohort and sufficient variability in BCs were used for MWU testing. Inserts represent motifs that lacked sufficient observations for MWU testing, but had $\log_2FC \geq 1$ and ≥ 5 hits.

(C–E) Single-cell transcriptomic data confirm a role for *Msc* during murine embryonic development.

(C) Re-analysis of MOCA data (Cao et al., 2019) identified 24 cell clusters at day E11.5.

(D) Expression levels for Musclin (*Msc*) in single-cell data from MOCA at E11.5 in cell clusters showed specific expression in myocytes (cell cluster 12 in C). Note: cluster numbers (x axis) correspond to cell cluster numbers in the UMAP plot in (C).

(E) Single-cell expression data of different cell clusters of the lambdoidal junction at E11.5 are shown as dot plot. For each cell cluster, the percentage of cells expressing *Msc* is indicated by dot size, while the average expression level is indicated by color. This illustrates expression of *Msc* in palatal epithelium and maxillary prominences.

(F) Nine DNMs mapped to the MSC motif (MA0665.1; seven in nsCL/P and two in NCR cohort). The sequences of the nine regions are illustrated per genomic region, as sorted according to BC, and with colored dots highlighting the cohort in which they were observed. At each position of a DNM, the allelic change is indicated in the order ref/alt.

molecular pathways through their location in transcription factor binding sites (TFBSs). Based on 28,773 DNMs and 810 PWMs, a total of 119,275 DNM-PWM hits were observed in the entire cohort. These pairs included 710 different PWMs and 21,043 DNMs (i.e., for 73.1% of the analyzed DNMs, the respective genomic context was located at a binding site of at least one PWM; Figure S11). After stringent filtering (supplemental methods), 88,129 DNM-PWM hits remained in the analysis. These showed a similar distribution in

both cohorts (37,695 in nsCL/P versus 50,434 in NCR, $p = 0.56$).

At the level of individual PWMs, we observed four TFs whose PWMs showed a nominally significant excess in the nsCL/P trios (Figure 3A, HES7/HES5/ATF3/MS; all $p < 0.05$), and a $\log_2FC \geq 1$. In addition, 24 PWMs were identified for which at least one TFBS was predicted at a DNM region in the nsCL/P cohort, but none in the NCR cohort. These motifs included TFs with an established role in craniofacial development, such as TFAP2alpha (vers.3;

4 DNMs in nsCL/P, none in NCR; insert [Figure 3A](#)). When we aimed at identifying TF motifs with a significant difference in binding change (as opposed to frequency), one nominally significant hit (MEF2A, $p = 0.03$) was observed, together with an additional set of 17 motifs that had $\log_2FC \geq 1$, but lacked the prerequisites for formal MWU calculations ([supplemental methods](#); [Figure 3B](#)). Seven TFs were shared between the two approaches, including TFs Musculin (MSC; [Table S27](#)) and Activating Transcription Factor 3 (ATF3; [Table S28](#)). Notably, MSC and ATF3 were the only of these seven TFs for which a nominally significant Fisher's exact test result was generated ([Table S29](#)), prioritizing them as candidate TFs.

Analyses of single-cell expression data support a role for Musculin

Next, analyses were performed to determine the expression of the orthologs for *MSC* ([MIM: 603628]; *Msc*) and *ATF3* (*Atf3*) in single-cell data from the developing mouse embryo during E9.5 to E13.5 (MOCA⁴³; Uniform Manifold Approximation and Projection [UMAP] plots in [Figure S12](#)). *Atf3* showed strong expression in endothelial cells, while being sparsely expressed in almost all other cell types ([Figure S13](#)). In contrast, our analyses revealed a specific expression pattern for *Msc* starting at E10.5. On day E10.5, *Msc* was expressed in sensory neurons but also in connective tissue progenitors and myocytes ([Figure S14](#)). Expression remained abundant in connective tissue progenitors, sensory neurons and myocytes on day E11.5 and was accompanied by expression in chondrocytes/osteoblasts and cardiac muscle lineage ([Figures 3C](#) and [3D](#)). On day E12.5, *Msc* was most expressed in neural progenitor cells but also in sensory neurons and jaw and tooth progenitors. On day E13.5 *Msc* was expressed mainly in neural progenitor cells ([Figure S14](#)). While the MOCA data provide information on global expression in whole embryonic mice, their resolution concerning specific facial tissues is limited. Therefore, additional analyses were performed on single-cell data from the murine lambdoidal junction at day E11.5. Again, this revealed a low, but anatomically specific, expression of *Msc*, particularly in the palatal epithelium and the anterior and medial maxillary prominences ([Figure 3E](#)), while expression of *Atf3* was restricted to monocytes/macrophages and endothelial cells of vasculature ([Figure S15](#)).

DNMs in MSC binding sites affect binding *in vitro*

Based on those findings, we focused on MSC as candidate TF for nsCL/P. Detailed inspection of the MSC binding motifs revealed that the seven DNMs in nsCL/P were located at more central positions within the motifs, compared with the only two DNMs in the NCR cohort ([Figure 3F](#); [Table S27](#)). To confirm that MSC binds to the predicted binding motif, and that binding is altered by the DNMs as predicted *in silico*, electrophoretic mobility shift assays (EMSAs) were performed for five selected DNMs, in triplicates.

For all five sequences, EMSA analysis confirmed the binding of MSC to either the reference and/or the alternative

motif ([Figure S16A](#); [Table S30](#)): for three of the five sequences, the observed direction of effect was consistent with predictions (i.e., gain of binding for chr. 16, loss of binding for chr. 5 and 10). For two regions, limited evidence was found for either any binding change at all (chr. 6), or the effect was observed in the opposite direction (chr. 7). Closer analysis of the respective genomic sequence revealed that, in the region of the DNM at chr. 7, a second MSC binding motif was present, which might have affected the prediction outcome ([Figure S16B](#)). The present data confirm that MSC binds to the predicted motif and suggest that this binding could be affected by mutations *in vitro*.

Discussion

WGS allows for a systematic investigation of genetic variants; i.e., across the allelic spectrum and variant types. Therefore, WGS data are a powerful resource to expand our understanding of susceptibility factors for nsCL/P, in particular when both coding and non-coding variants are analyzed jointly. However, the large number of rare variants in individual genomes challenges the identification of causal variants at the statistical level, and this is further hampered by our incomplete knowledge regarding regulatory processes occurring in the non-coding genome. In the present study, we analyzed DNMs as a specific class of variants, in a European-based nsCL/P cohort of 211 trios, and included both coding and non-coding variants in our investigation. While the cohort size is small compared with other traits of multifactorial etiology, it is similar to the cohort size included in the first nsCL/P GWAS that reported a genome-wide significant locus.⁴⁴ Three main findings emerged from our WGS study on nsCL/P.

First, while our study design included systematic approaches to enrich for true-positive signals, we failed to detect robust associations in our hypothesis-driven analyses. We observed some nominally significant findings, but these warrant further replication in order to allow for firm conclusions (in particular, for those findings that are based on singleton observations). Future studies including more trios and ethnicities but also additional control cohorts might be an important avenue to follow. The lack of systematic evidence in our study might indicate either that DNMs in the selected regions do not contribute to nsCL/P or that our analyses were statistically underpowered. Importantly, next to sample size, the power of our study might have been limited by the selection of the reference cohort, which comprised individuals with ES for which WGS data were generated within the same project. While this is a technical advantage for comparative analyses, some epidemiological data have suggested some shared etiology between OFC and cancer in general.⁴⁵ Still, so far, no evidence is available for a shared etiology between ES and nsCL/P from epidemiological or molecular data.² Furthermore, most current *in silico* prediction scores are trained on input data that are biased for deleterious

protein-coding variants and, therefore, are ineffective for non-coding regions. This limits their usage for WGS data, as illustrated in our study by the comparably low number of observed non-coding DNMs with high CADD scores.

Second, despite the limited evidence for overall enrichments, we identified a convergence of DNMs at loci that had prior evidence for an involvement in nsCL/P. Most interestingly, we observed a significant overrepresentation of DNMs in regions that were previously implicated in nsCL/P etiology by common variants. Specifically, two risk loci, 4q28 and 2p21_{PKDCC}, harbored significantly more DNMs in nsCL/P trios than the reference cohort. At 2p21, the variants clustered within a region of 175 kb, in close vicinity to rs6740960, which has been suggested as the sole causal variant at this locus.^{39,46} As another example, we observed two intronic DNMs in the nsCL/P candidate gene, *ZFH4*,¹¹ for which a frameshift mutation was previously reported (Table S31). While the exact functional effect and molecular mechanisms of these non-coding DNMs at GWAS loci or within candidate gene loci remain unclear, these findings illustrate the presence of allelic heterogeneity at established loci and pave the way for functional follow-up studies.

Finally, our results suggest that differential binding of Musculin (*MSC*, or *MyoR*) to its binding sequence might be of relevance to nsCL/P etiology. *MSC* is a basic-helix-loop-helix TF that is involved in the development of orofacial branchiomeric muscles (OBMs).⁴⁷ Interestingly, previous studies have identified sub-epithelial alterations in a specific OBM type, *musculus orbicularis oris*, as a subclinical phenotype in the relatives of individuals with nsCL/P, and these alterations are considered an intermediate phenotype of nsCL/P.^{48–51} Notably, the network of TFs regulating OBM development includes several TFs that are encoded by genes implicated in nsCL/P via their presence at GWAS risk loci; i.e., *NOG* (MIM: 602991),⁵² *PAX7* (MIM: 167410),⁵³ *FGF10* (MIM: 602115),⁴ and *GREM1* (MIM: 603054)⁵⁴ (Figure S17). However, the exact coordination of this gene regulatory network and the context-specific effects of the binding changes remain unclear at the moment and require further investigation.

In summary, we here provide a genome-wide analysis of DNMs in nsCL/P that includes variation in the non-coding genome. While our study illustrates the challenges associated with our understanding of non-coding variation, we also provide evidence for causal DNMs at nsCL/P GWAS loci and suggest that common and rare variants in the muscle developmental pathway might be involved in nsCL/P etiology.

Data and code availability

Original data concerning the present genetic and functional analyses can be accessed as follows: WGS data for nsCL/P and NCR cohorts are available at dbGaP phs001168.v1.p1 and phs001228.v1.p1, respectively. Chromatin state segmentation data for craniofacial tissue (CT) are available at Gene Expression Omnibus (GEO), under accession number GSE97752. Chromatin state segmentation data for

hNCC and cNCC are available at Zenodo (<https://doi.org/10.5281/zenodo.3911187>). CNEs are available on GitHub (<https://github.com/pjshort/DDDNonCoding2017/tree/master/data>). Original data of TADs are available at GEO under accession number GSE35156. Original data for single-cell expression from whole mouse embryos are available under <https://oncoscape.v3.sttrcancer.org/atlas.gs.washington.edu.mouse.rna/downloads> (Processed/Sampled/Split Data; gene_count_cleaned.RDS). Single-cell expression data for the lambdaoid junction are available at GEO under accession number GSM3867275. The accession number for the code of the modified version of denovoLOBGOB reported in this paper is publicly available at Zenodo (<https://doi.org/10.5281/zenodo.5601707>).

Supplemental information

Supplemental information can be found online at <https://doi.org/10.1016/j.xhgg.2022.100166>.

Acknowledgments

This work was supported by the German Research Council through funding provided to K.U.L. (DFG; LU 1944/3-1). H.K.Z. received support from the BONFOR program of the Medical Faculty Bonn (SciMed program, O-149.0132).

The present results were obtained using data generated by the Gabriella Miller Kids First (GMKF) Pediatric Research Program projects phs001168.v1.p1 and phs001228.v1.p1. Upon approved data access, data were downloaded from dbGaP (www.ncbi.nlm.nih.gov/gap) and the Website of the GMKF project (<https://kidsfirstdrf.org>). The GMKF Website and the Kids First Data Resource Center are supported by the National Institutes of Health (NIH) Common Fund (U2CHL138346). European nsCL/P trios were sequenced at Washington University's Mc Donnell Genome Institute (X01-HL132363, with principal investigators M.L.M. and E.F.) and this project was supported by the NIH through the following funding sources: R01-DE016148 (M.L.M. and S.M.W.), R01-DE014581 (T.H.B.), and R01-DD000295 (G.L.W.). Ewing sarcoma trios as NCR cohort were recruited within the context of the Children's Oncology Group AEPI10N5 Study (Genetic Epidemiology of Ewing Sarcoma, NCT01876303) and sequenced within the GMKF Ewing Sarcoma project (X01-HL132385, with principal investigator J.D.S.). The Ewing Sarcoma study was supported by the Children's Oncology Group and the National Cancer Institute.

Author contributions

H.K.Z. and K.U.L. conceptualized the study and acquired funding. H.K.Z., A. Schmidt, M.H., F.T., F.U.B., J.W., D.B., and P.M.K. analyzed sequencing data and/or provided computational resources. L.W. and H.K.Z. planned and performed statistical analyses. H.K.Z., L.W., A. Schmidt, A. Siewert, A.B.S., E.M., N.L., and K.U.L. jointly interpreted data. A. Siewert designed and performed the analysis of single-cell expression data. H.K.Z., S.A.J., and K.P. designed, performed, and interpreted EMSA experiments. H.K.Z. wrote the first version of the manuscript with contributions by L.W., A. Siewert, K.P., and K.U.L. All authors edited and approved the final manuscript.

Declaration of interests

The authors declare no competing interests.

Web resources

GMKF Pediatric Research Program, www.commonfund.nih.gov/KidsFirst

denovoLOBOG, <https://github.com/pjshort/denovoTF>.
FunciVar, <https://github.com/Simon-Coetzee/funcivar>.
GEO, <https://www.ncbi.nlm.nih.gov/geo/>
GENCODE, https://www.encodegenes.org/human/grc_h37_mapped_releases.html.

GnomAD v3.1., <https://gnomad.broadinstitute.org/>
JASPAR 2020, <https://bioconductor.org/packages/release/data/annotation/html/JASPAR2020.html>.

MOCA, <https://oncoscape.v3.sttrcancer.org/atlas.gs.washington.edu.mouse.rna/landing>.

OMIM, <http://www.omim.org/>.

TFBSTools, <http://bioconductor.org/packages/release/bioc/html/TFBSTools.html>.

Ensembl Variant Effect Predictor, <https://www.ensembl.org/info/docs/tools/vep/online/input.html>.

VISTA Enhancer Browser, <https://enhancer.lbl.gov/>

References

- Mangold, E., Ludwig, K.U., and Nöthen, M.M. (2011). Breakthroughs in the genetics of orofacial clefting. *Trends Mol. Med.* 17, 725–733.
- Christensen, K., Juel, K., Herskind, A.M., and Murray, J.C. (2004). Long term follow up study of survival associated with cleft lip and palate at birth. *BMJ* 328, 1405.
- Grosen, D., Bille, C., Petersen, I., Skytthe, A., Hjelmborg, J.v.B., Pedersen, J.K., Murray, J.C., and Christensen, K. (2011). Risk of oral clefts in twins. *Epidemiology* 22, 313–319.
- Welzenbach, J., Hammond, N.L., Nikolić, M., Thieme, F., Ishorst, N., Leslie, E.J., Weinberg, S.M., Beaty, T.H., Marazita, M.L., Mangold, E., et al. (2021). Integrative approaches generate insights into the architecture of non-syndromic cleft lip ± cleft palate. *HGG Adv.* 2, 100038.
- Basha, M., Demeer, B., Revencu, N., Helaers, R., Theys, S., Bou Saba, S., Boute, O., Devauchelle, B., Francois, G., Bayet, B., et al. (2018). Whole exome sequencing identifies mutations in 10% of patients with familial non-syndromic cleft lip and/or palate in genes mutated in well-known syndromes. *J. Med. Genet.* 55, 449–458.
- Cox, L.L., Cox, T.C., Moreno Uribe, L.M., Zhu, Y., Richter, C.T., Nidey, N., Standley, J.M., Deng, M., Blue, E., Chong, J.X., et al. (2018). Mutations in the epithelial cadherin-p120-catenin complex cause mendelian non-syndromic cleft lip with or without cleft palate. *Am. J. Hum. Genet.* 102, 1143–1157.
- Savastano, C.P., Brito, L.A., Faria, Á.C., Setó-Salvia, N., Peskett, E., Musso, C.M., Alvizi, L., Ezquina, S.A.M., James, C., GOS-gene, et al. (2017). Impact of rare variants in ARHGAP29 to the etiology of oral clefts: role of loss-of-function vs missense variants. *Clin. Genet.* 91, 683–689.
- Butali, A., Mossey, P., Adeyemo, W., Eshete, M., Gaines, L., Braimah, R., Aregbesola, B., Rigdon, J., Emeka, C., Olutayo, J., et al. (2014). Rare functional variants in genome-wide association identified candidate genes for nonsyndromic clefts in the African population. *Am. J. Med. Genet. Part A* 164A, 2567–2571.
- Letra, A., Maili, L., Mulliken, J.B., Buchanan, E., Blanton, S.H., and Hecht, J.T. (2014). Further evidence suggesting a role for variation in ARHGAP29 variants in nonsyndromic cleft lip/palate. *Birth Defects Res. A Clin. Mol. Teratol.* 100, 679–685.
- Leslie, E.J., Taub, M.A., Liu, H., Steinberg, K.M., Koboldt, D.C., Zhang, Q., Carlson, J.C., Hetmanski, J.B., Wang, H., Larson, D.E., et al. (2015). Identification of functional variants for cleft lip with or without cleft palate in or near PAX7, FGFR2, and NOG by targeted sequencing of GWAS loci. *Am. J. Hum. Genet.* 96, 397–411.
- Bishop, M.R., Diaz Perez, K.K., Sun, M., Ho, S., Chopra, P., Mukhopadhyay, N., Hetmanski, J.B., Taub, M.A., Moreno-Urbe, L.M., Valencia-Ramirez, L.C., et al. (2020). Genome-wide enrichment of de novo coding mutations in orofacial cleft trios. *Am. J. Hum. Genet.* 107, 124–136.
- Fakhouri, W.D., Rahimov, F., Attanasio, C., Kouwenhoven, E.N., Ferreira De Lima, R.L., Felix, T.M., Nitschke, L., Huver, D., Barrons, J., Kousa, Y.A., et al. (2014). An etiologic regulatory mutation in IRF6 with loss- and gain-of-function effects. *Hum. Mol. Genet.* 23, 2711–2720.
- Cvjetkovic, N., Maili, L., Weymouth, K.S., Hashmi, S.S., Mulliken, J.B., Topczewski, J., Letra, A., Yuan, Q., Blanton, S.H., Swindell, E.C., et al. (2015). Regulatory variant in FZD6 gene contributes to nonsyndromic cleft lip and palate in an African-American family. *Mol. Genet. Genomic Med.* 3, 440–451.
- Morris, V.E., Hashmi, S.S., Zhu, L., Maili, L., Urbina, C., Blackwell, S., Greives, M.R., Buchanan, E.P., Mulliken, J.B., Blanton, S.H., et al. (2020). Evidence for craniofacial enhancer variation underlying nonsyndromic cleft lip and palate. *Hum. Genet.* 139, 1261–1272.
- Shaffer, J.R., LeClair, J., Carlson, J.C., Feingold, E., Buxó, C.J., Christensen, K., Deleyiannis, F.W.B., Field, L.L., Hecht, J.T., Moreno, L., et al. (2019). Association of low-frequency genetic variants in regulatory regions with nonsyndromic orofacial clefts. *Am. J. Med. Genet. Part A* 179, 467–474.
- Kircher, M., Witten, D.M., Jain, P., O’Roak, B.J., Cooper, G.M., and Shendure, J. (2014). A general framework for estimating the relative pathogenicity of human genetic variants. *Nat. Genet.* 46, 310–315.
- Smedley, D., Schubach, M., Jacobsen, J.O.B., Köhler, S., Zemojtel, T., Spielmann, M., Jäger, M., Hochheiser, H., Washington, N.L., McMurry, J.A., et al. (2016). A whole-genome analysis framework for effective identification of pathogenic regulatory variants in mendelian disease. *Am. J. Hum. Genet.* 99, 595–606.
- Shihab, H.A., Rogers, M.F., Gough, J., Mort, M., Cooper, D.N., Day, I.N.M., Gaunt, T.R., and Campbell, C. (2015). An integrative approach to predicting the functional effects of non-coding and coding sequence variation. *Bioinformatics* 31, 1536–1543.
- Quang, D., Chen, Y., and Xie, X. (2015). DANN: a deep learning approach for annotating the pathogenicity of genetic variants. *Bioinformatics* 31, 761–763.
- Huang, Y.F., Gulko, B., and Siepel, A. (2017). Fast, scalable prediction of deleterious noncoding variants from functional and population genomic data. *Nat. Genet.* 49, 618–624.
- Wells, A., Heckerman, D., Torkamani, A., Yin, L., Sebat, J., Ren, B., Telenti, A., and di Iulio, J. (2019). Ranking of non-coding

- pathogenic variants and putative essential regions of the human genome. *Nat. Commun.* *10*, 5241.
22. McLaren, W., Gil, L., Hunt, S.E., Riat, H.S., Ritchie, G.R.S., Thormann, A., Flicek, P., and Cunningham, F. (2016). The Ensembl variant effect predictor. *Genome Biol.* *17*, 122.
 23. Jones, M.R., Peng, P.C., Coetzee, S.G., Tyrer, J., Reyes, A.L.P., Corona, R.I., Davis, B., Chen, S., Dezem, F., Seo, J.H., et al. (2020). Ovarian cancer risk variants are enriched in histotype-specific enhancers and disrupt transcription factor binding sites. *Am. J. Hum. Genet.* *107*, 622–635.
 24. Rada-Iglesias, A., Bajpai, R., Prescott, S., Brugmann, S.A., Swigut, T., and Wysocka, J. (2012). Epigenomic annotation of enhancers predicts transcriptional regulators of human neural crest. *Cell Stem Cell* *11*, 633–648.
 25. Prescott, S.L., Srinivasan, R., Marchetto, M.C., Grishina, I., Narvaiza, I., Selleri, L., Gage, F.H., Swigut, T., and Wysocka, J. (2015). Enhancer divergence and cis-regulatory evolution in the human and chimp neural crest. *Cell* *163*, 68–83.
 26. Wilderman, A., VanOudenhove, J., Kron, J., Noonan, J.P., and Cotney, J. (2018). High-resolution epigenomic Atlas of human embryonic craniofacial development. *Cell Rep.* *23*, 1581–1597.
 27. Short, P.J., McRae, J.F., Gallone, G., Sifrim, A., Won, H., Geschwind, D.H., Wright, C.F., Firth, H.V., FitzPatrick, D.R., Barrett, J.C., et al. (2018). De novo mutations in regulatory elements in neurodevelopmental disorders. *Nature* *555*, 611–616.
 28. Visel, A., Minovitsky, S., Dubchak, I., and Pennacchio, L.A. (2007). VISTA Enhancer Browser—a database of tissue-specific human enhancers. *Nucleic Acids Res.* *35*, D88–D92.
 29. Fornes, O., Castro-Mondragon, J.A., Khan, A., van der Lee, R., Zhang, X., Richmond, P.A., Modi, B.P., Correard, S., Gheorghie, M., Baranašić, D., et al. (2020). JASPAR 2020: update of the open-access database of transcription factor binding profiles. *Nucleic Acids Res.* *48*, D87–D92.
 30. Li, H., Jones, K.L., Hooper, J.E., and Williams, T. (2019). The molecular anatomy of mammalian upper lip and primary palate fusion at single cell resolution. *Development* *146*, dev174888.
 31. Kong, A., Frigge, M.L., Masson, G., Besenbacher, S., Sulem, P., Magnusson, G., Gudjonsson, S.A., Sigurdsson, A., Jonasdottir, A., Jonasdottir, A., et al. (2012). Rate of de novo mutations and the importance of father's age to disease risk. *Nature* *488*, 471–475.
 32. Warner, D.R., Smith, H.S., Webb, C.L., Greene, R.M., and Pisano, M.M. (2009). Expression of Wnts in the developing murine secondary palate. *Int. J. Dev. Biol.* *53*, 1105–1112.
 33. Geetha-Loganathan, P., Nimmagadda, S., Antoni, L., Fu, K., Whiting, C.J., Francis-West, P., and Richman, J.M. (2009). Expression of WNT signalling pathway genes during chicken craniofacial development. *Dev. Dyn.* *238*, 1150–1165.
 34. Iyyanar, P.P.R., and Nazarali, A.J. (2017). *Hoxa2* inhibits bone morphogenetic protein signaling during osteogenic differentiation of the palatal mesenchyme. *Front. Physiol.* *8*, 929.
 35. Nie, S., Kee, Y., and Bronner-Fraser, M. (2009). Myosin-X is critical for migratory ability of *Xenopus* cranial neural crest cells. *Dev. Biol.* *335*, 132–142.
 36. Hwang, Y.S., Luo, T., Xu, Y., and Sargent, T.D. (2009). Myosin-X is required for cranial neural crest cell migration in *Xenopus laevis*. *Dev. Dyn.* *238*, 2522–2529.
 37. Bachg, A.C., Horsthemke, M., Skryabin, B.V., Klasen, T., Nagelmann, N., Faber, C., Woodham, E., Machesky, L.M., Bachg, S., Stange, R., et al. (2019). Phenotypic analysis of *Myo10* knockout (*Myo10tm2/tm2*) mice lacking full-length (motorized) but not brain-specific headless myosin X. *Sci. Rep.* *9*, 597.
 38. Dixon, J.R., Selvaraj, S., Yue, F., Kim, A., Li, Y., Shen, Y., Hu, M., Liu, J.S., and Ren, B. (2012). Topological domains in mammalian genomes identified by analysis of chromatin interactions. *Nature* *485*, 376–380.
 39. Ludwig, K.U., Böhmer, A.C., Bowes, J., Nikolić, M., Ishorst, N., Wyatt, N., Hammond, N.L., Gözl, L., Thieme, F., Barth, S., et al. (2017). Imputation of orofacial clefting data identifies novel risk loci and sheds light on the genetic background of cleft lip ± cleft palate and cleft palate only. *Hum. Mol. Genet.* *26*, 829–842.
 40. Yu, Y., Zuo, X., He, M., Gao, J., Fu, Y., Qin, C., Meng, L., Wang, W., Song, Y., Cheng, Y., et al. (2017). Genome-wide analyses of non-syndromic cleft lip with palate identify 14 novel loci and genetic heterogeneity. *Nat. Commun.* *8*, 14364.
 41. Imuta, Y., Nishioka, N., Kiyonari, H., and Sasaki, H. (2009). Short limbs, cleft palate, and delayed formation of flat proliferative chondrocytes in mice with targeted disruption of a putative protein kinase gene, *Pkdcc* (AW548124). *Dev. Dyn.* *238*, 210–222.
 42. Melvin, V.S., Feng, W., Hernandez-Lagunas, L., Artinger, K.B., and Williams, T. (2013). A morpholino-based screen to identify novel genes involved in craniofacial morphogenesis. *Dev. Dyn.* *242*, 817–831.
 43. Cao, J., Spielmann, M., Qiu, X., Huang, X., Ibrahim, D.M., Hill, A.J., Zhang, F., Mundlos, S., Christiansen, L., Steemers, F.J., et al. (2019). The single-cell transcriptional landscape of mammalian organogenesis. *Nature* *566*, 496–502.
 44. Birnbaum, S., Ludwig, K.U., Reutter, H., Herms, S., Steffens, M., Rubini, M., Baluardo, C., Ferrian, M., Almeida De Assis, N., Alblas, M.A., et al. (2009). Key susceptibility locus for non-syndromic cleft lip with or without cleft palate on chromosome 8q24. *Nat. Genet.* *41*, 473–477.
 45. Bille, C., Winther, J.F., Bautz, A., Murray, J.C., Olsen, J., and Christensen, K. (2005). Cancer risk in persons with oral cleft - a population-based study of 8, 093 cases. *Am. J. Epidemiol.* *161*, 1047–1055.
 46. Mohammed, J., Arora, N., Matthews, H.S., Hansen, K., Bader, M., Weinberg, S.M., Swigut, T., Claes, P., Selleri, L., Wysocka, J., et al. (2022). A common cis-regulatory variant impacts normal-range and disease-associated human facial shape through regulation of *PKDCC* during chondrogenesis. Preprint at bioRxiv. <https://doi.org/10.1101/2022.09.05.506587>.
 47. Rosero Salazar, D.H., Carvajal Monroy, P.L., Wagener, F.A.D.T.G., and Von den Hoff, J.W. (2020). Orofacial muscles: embryonic development and regeneration after injury. *J. Dent. Res.* *99*, 125–132.
 48. Weinberg, S.M., Neiswanger, K., Martin, R.A., Mooney, M.P., Kane, A.A., Wenger, S.L., Losee, J., Deleyiannis, E., Ma, L., De Salamanca, J.E., et al. (2006). The Pittsburgh Oral-Facial Cleft study: expanding the cleft phenotype. Background and justification. *Cleft Palate. Craniofac. J.* *43*, 7–20.
 49. Martin, R.A., Hunter, V., Neufeld-Kaiser, W., Flodman, P., Spence, M.A., Furnas, D., and Martin, K.A. (2000). Ultrasonographic detection of orbicularis oris defects in first degree relatives of isolated cleft lip patients. *Am. J. Med. Genet.* *90*, 155–161.
 50. Neiswanger, K., Weinberg, S.M., Rogers, C.R., Brandon, C.A., Cooper, M.E., Bardi, K.M., Deleyiannis, F.W.B., Resick, J.M., Bowen, A., Mooney, M.P., et al. (2007). Orbicularis oris muscle defects as an expanded phenotypic feature in nonsyndromic

- cleft lip with or without cleft palate. *Am. J. Med. Genet. Part A* *143A*, 1143–1149.
51. Marazita, M.L. (2007). Subclinical features in non-syndromic cleft lip with or without cleft palate (CL/P): review of the evidence that subepithelial orbicularis oris muscle defects are part of an expanded phenotype for CL/P. *Orthod. Craniofac. Res.* *10*, 82–87.
 52. Mangold, E., Ludwig, K.U., Birnbaum, S., Baluardo, C., Ferrian, M., Herms, S., Reutter, H., de Assis, N.A., Chawa, T.A., Mattheisen, M., et al. (2010). Genome-wide association study identifies two susceptibility loci for nonsyndromic cleft lip with or without cleft palate. *Nat. Genet.* *42*, 24–26.
 53. Ludwig, K.U., Mangold, E., Herms, S., Nowak, S., Reutter, H., Paul, A., Becker, J., Herberz, R., AlChawa, T., Nasser, E., et al. (2012). Genome-wide meta-analyses of nonsyndromic cleft lip with or without cleft palate identify six new risk loci. *Nat. Genet.* *44*, 968–971.
 54. Ludwig, K.U., Ahmed, S.T., Böhmer, A.C., Sangani, N.B., Varghese, S., Klamt, J., Schuenke, H., Gültepe, P., Hofmann, A., Rubini, M., et al. (2016). Meta-analysis reveals genome-wide significance at 15q13 for nonsyndromic clefting of both the lip and the palate, and functional analyses implicate *GREM1* as a plausible causative gene. *PLoS Genet.* *12*, e1005914.